PERGAMON

International Journal of Heat and Mass Transfer 44 (2001) 525–536

International Journal of HEAT and MASS TRANSFER

www.elsevier.com/locate/ijhmt

Vertical mixing above a steady circular source of buoyancy

Michael Epstein, James P. Burelbach*

Fauske and Associates Inc., 16W070 West 83rd Street, Burr Ridge, IL 60521, USA

Received 10 December 1999; received in revised form 25 March 2000

Abstract

Experiments using water and brine were performed to simulate the mixing pattern above a slow steady circular release of light fuel gas into a region of otherwise quiescent, heavier air. The experiments reveal the existence of a horizontal inward moving boundary- or mixing-layer flow above the release surface. Over the central region of the release area the mixing layer turns upward and feeds a vertical buoyant plume. Measured mixing layer thicknesses and solute salt concentrations were compared with predictions based on a concentration boundary-layer type model combined with a model for vertical flow into the plume.

1. Introduction

This paper addresses the slow release of a light fuel gas into a heavier, quiescent ambient gas (air) environment. The study is stimulated by the need for assessing the flammability hazard in the headspaces of certain process waste storage tanks during episodic light fuel gas releases from the stored sludge/supernate. In that situation the release area is considerably smaller than the waste surface area. The density difference between the release gas and the surrounding air, combined with the very low initial momentum of the release, causes the release gas to move inward to the center of the release area in the form of a horizontal boundary layer, mixing layer, or 'floor plume' (hereafter referred to as the mixing layer). Ultimately, the radial inward flow turns sharply upward and feeds a vertical buoyant plume. A similar turbulent mixing layer/vertical plume structure occurs above large-area pool fires, and a useful review of this subject has been provided by Delichatsios [1]. Horizontal free-convection boundary layers capped by a vertical plume have been observed on upward facing heated disks [2], although the laboratory scale horizontal layer in that situation is thin, and the flow within it is usually laminar.

The salt-water modeling technique is used in this study to investigate the mixing layer shape and to determine the extent to which the released fluid is diluted (or concentrated) by the heavier ambient fluid. Fresh water is injected upward at very low velocity through a circular porous plate into a tank containing heavier brine. The measured mixing layer thickness and the salt concentrations are compared with theoretical predictions based on the solutions to two simplified integral models: a concentration boundary-layer type model for the mixing layer and a model for the vertical plume. The models are joined at the 'neck' location where the mixing layer changes to the plume. In the prediction of the mixing layer's behavior the vertical mixing mechanism is the critical element: the conservation equations are not complete unless a realistic model of buoyancy-driven turbulent mixing is adopted.

The theory presented here uses the concept of a vertical diffusion (or dispersion) coefficient to model the upward transport of the lighter fluid (fresh water)

* Corresponding author. Tel.: +1-630-3238750; fax: +1-630-9865481.

E-mail address: burelbach@fauske.com (J.P. Burelbach).

0017-9310/01/$ - see front matter
PII: S0017-9310(00)00134-4

Nomenclature

E dispersion coefficient for vertical mixing
E_0 entrainment coefficient for plume (0.12)
Fr_p Froude number for plume; Eq. (35)
Fr Froude number for release; $v_0/\sqrt{2gR_0(\rho_\infty-\rho_0)/\rho_\infty}$
g gravitational acceleration (m s^{-2})
k constant of proportionality in isothermal salt solution equation of state (0.64 for NaCl solute); Eq. (12)
ℓ characteristic mixing length for turbulent diffusion (m)
M_H molecular weight of pure ambient gas (kg $kmol^{-1}$)
M_L molecular weight of pure light release gas (kg $kmol^{-1}$)
$M_{L,p}$ molecular weight of gas mixture at neck (kg $kmol^{-1}$)
P local dynamic pressure within mixing layer (N m^{-2})
Q inward volumetric flow of fluid within mixing layer (m^3 s^{-1})
Q_p volumetric flow of fluid from mixing layer into plume (at neck) (m^3 s^{-1})
Q_0 volumetric flow of injected fluid (fresh water) at release surface (m^3 s^{-1})
r radial coordinate in mixing layer or plume (m)
R radius of plume (m)
R_p neck radius (m)
R_0 radius of circular release area or porous disk in brine/water tests (m)
R_2 radial location of sampling point 2 (m)
u horizontal (radial) velocity component in mixing layer (m s^{-1})
$\bar{u}$ average radial velocity at location r in mixing layer (m s^{-1})
u_e entrainment velocity in plume model (m s^{-1})
v vertical velocity component in plume (m s^{-1})
v_p vertical mixture velocity at neck (m s^{-1})
v_0 superficial velocity of injected fluid (fresh water) at release surface (m s^{-1})
x dummy integration variable
Y local solute (salt) mass fraction (ρ_s/ρ)
Y_∞ ambient solute (salt) mass fraction
$\overline{Y}$ average salt mass fraction at location r in mixing layer
Y_i salt mass fraction at sampling point i
$\bar{Y}_L$ average light (fuel) gas mass fraction at location r in mixing layer
Y_p average solute (salt) mass fraction at neck
z vertical coordinate in mixing layer or plume (m)
Z dimensionless vertical distance in plume

Greek symbols
β mixing-length-thickness proportionality coefficient
δ vertical thickness of mixing layer (m)
λ dimensionless plume flow rate; Eq. (33)
ξ transformation variable
ρ local density of mixture (kg m^{-3})
ρ_H density of pure ambient gas (kg m^{-3})
ρ_i brine density at sampling point i (kg m^{-3})
ρ_0 density of pure water (kg m^{-3})
ρ_p mixture density at neck (kg m^{-3})
ρ_s salt concentration (kg m^{-3})
$\rho_{s,p}$ salt concentration at neck (kg m^{-3})
$\rho_{s,\infty}$ ambient salt concentration (kg m^{-3})
ρ_∞ density of ambient fluid (kg m^{-3})

through the heavier fluid (brine) within the mixing layer. In particular, this approach adopts the vertical dispersion coefficient law proposed by Baird and Rice [3] for steady-state vertical mixing in spray and bubble columns, and later modified by Holmes et al. [4] to deal with the upward turbulent transport of a lighter fluid through a heavier miscible fluid. Until now almost all of the experimental work performed on buoyancy-driven vertical mixing was carried out in high-aspect ratio tubes (or columns), and the mixing length required by the Baird–Rice dispersion coefficient law was found to be a constant proportional to the column diameter [4–8]. Recently, the authors [9] measured the depth of a wide (low-aspect ratio) brine/water mixing layer as a function of time and obtained a good correlation by employing a Baird–Rice mixing length that is proportional to the instantaneous thickness of the mixing layer. As will be seen, the steady-state mixing layer of interest here is of considerable lateral extent so that it would seem reasonable to assume that the mixing length is proportional to the local depth of the mixing layer. Indeed, this choice with a mixing length proportionality coefficient that is almost identical to the one inferred from the earlier, transient brine/water mixing study [9], yields reasonable agreement with the brine/water experimental data obtained in the present study on steady buoyant releases.

2. Theoretical model

In the experiments described below, water is injected with velocity v_0 through a porous disk of radius R_0 into a tank containing heavier brine. This disk is fastened to the bottom of the brine tank, and its area is small compared with that of the tank floor. The freshwater injected flow is assumed to be spatially uniform over the surface of the disk, and its volumetric flow rate is denoted by the symbol Q_0. Turbulent diffusional mixing between the ambient brine and the injected fresh water first occurs within a 'mixing' boundary layer of radially inward flow. This radial flow ultimately turns upward as it approaches the center of the release zone and feeds a vertical plume within which the mixing process continues. The combined mixing layer/plume flow is illustrated in Fig. 1. Initially the analysis is limited to the mixing region above the release disk and below the plume. In particular, attention is focused on the radial region $R_p < r < R_0$. It is desired to develop practical formulas (correlations) for the average solute (salt) concentration within the mixing layer and at the 'neck' of the mixing layer/plume configuration. It is also of interest to determine the shape of the mixing layer and identify where it changes to plume flow. To accomplish these goals, models of both the mixing layer and the plume flow are required.

2.1. Mixing layer

The following assumptions are introduced to model the mixing layer:

1. The mixing layer is treated as an isothermal, concentration boundary layer within which turbulent mixing between the injected fresh water and the overlying brine occurs mainly in the vertical z direction. Mixing in the radial r direction is ignored.
2. The effective diffusion coefficient E for vertical mixing is well-represented by the Baird and Rice [3] dispersion coefficient formula for the upward turbulent transport of a lighter fluid through a heavier miscible fluid [4,5]:

$$E = \ell^2 \left(\frac{g}{\rho} \frac{\partial \rho}{\partial z} \right)^{1/2} \tag{1}$$

3. Based on the previous study on unsteady vertical mixing in a wide layer [9], the characteristic mixing length ℓ in Eq. (1) is simply expressed as

$$\ell = \beta \, \delta(r) \tag{2}$$

where, $\delta(r)$ is the local depth (see Fig. 1) and β is a constant of about 0.16.

4. The boundary layer equations are simplified by the Boussinesq approximation and by the assumption

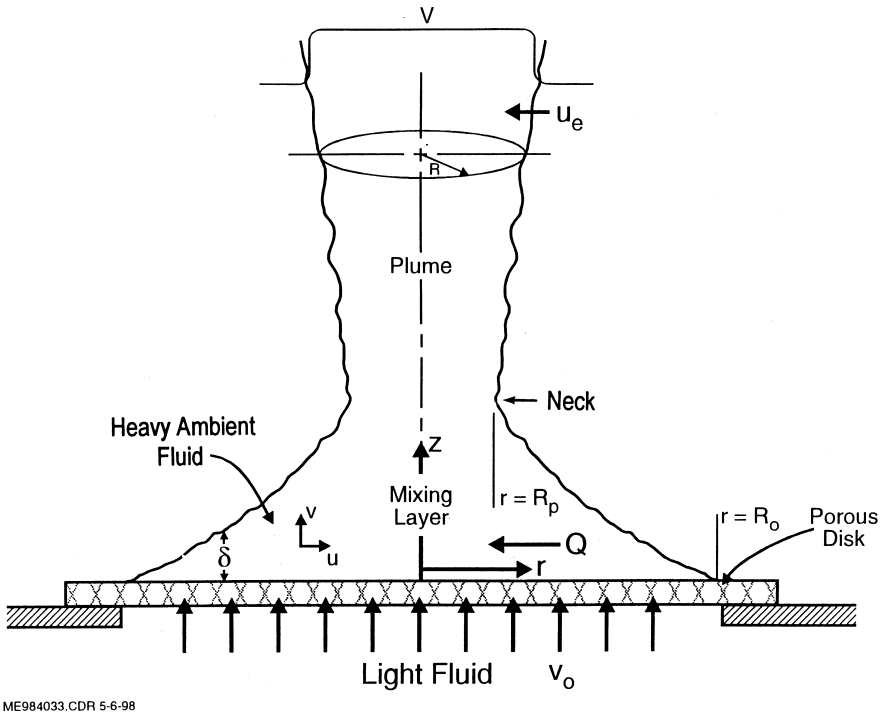

Fig. 1. Schematic of mixing layer capped by central plume, indicating flow direction and nomenclature.

that the concentration of the diffusing solute (salt) species is relatively low.

5. The horizontal (r-component) momentum equation and the solute species continuity equation are solved by an approximate integral method. The following simple analytical forms are assumed for the vertical solute concentration and velocity profiles, respectively:

$$Y(r,z) = Y_\infty - [Y_\infty - Y(r,0)]\left[\frac{\delta(r)-z}{\delta(r)}\right]^2 \tag{3}$$

$$u(r,z) = -\bar{u}(r) \tag{4}$$

where, the over-bar designates a vertical distance-averaged velocity, and the minus sign in Eq. (4) signifies inward radial flow. Eq. (3) describes a parabolic profile, while Eq. (4) represents plug flow. It is also convenient (and practical) to define a vertically averaged salt mass fraction,

$$\bar{Y}(r) = \frac{1}{\delta}\int_0^\infty Y(r,z)\mathrm{d}z = Y_\infty - \frac{1}{3}[Y_\infty - Y(r,0)] \tag{5}$$

6. Momentum boundary layer effects are ignored, and the inward uniform flow $\bar{u}(r)$ across the thickness of the mixing layer is driven solely by the radial buoyancy force established by the injection of light fluid.

Subject to these assumptions, the governing steady-state equations for $\delta(r)$, $\bar{u}(r)$ and $\bar{Y}(r)$ are the vertical component of the momentum equation,

$$\frac{\partial P}{\partial z} = (\rho - \rho_\infty)g \tag{6}$$

the integral form of the horizontal component of the momentum equation,

$$\frac{\mathrm{d}}{\mathrm{d}r}(r\bar{u}^2\delta) = \frac{r}{\rho}\frac{\mathrm{d}}{\mathrm{d}r}\int_0^\delta P\,\mathrm{d}z \tag{7}$$

and the integral form of the solute continuity equation,

$$\frac{\mathrm{d}}{\mathrm{d}r}[r\bar{u}\delta(Y_\infty - \bar{Y})] = -rv_0 Y_\infty \tag{8}$$

The boundary conditions for Eqs. (6)–(8) are

$$P = 0 \text{ at } z = \delta \quad \text{and } \delta = \bar{u} = 0 \text{ at } r = R_0 \tag{9}$$

At the porous release-surface ($z = 0$) the boundary condition is

$$\rho_0 v_0 Y(r,0) = \rho E(r,0)\frac{\partial Y}{\partial z}(r,0) \tag{10}$$

which states that the solute salt cannot pass through the porous disk. That is, the convective flux of salt due to the upward injection of fresh water is equal to the downward turbulent diffusion flux of salt to the porous surface. It can be shown with the results of the present formulation that, when the release Froude number is small ($Fr \lesssim 0.05$), the difference between $Y(r,0)$ in Eq. (10) evaluated away from the edge of the release and the ambient salt concentration Y_∞ is small enough that Y_∞ may replace $Y(r,0)$ on the left-hand side of Eq. (10). Admittedly, this statement is not quite true for some of the laboratory scale high-injection releases investigated here, for which the Froude number approaches 0.05. Nevertheless, it is felt that the convenient functional forms obtained for $\bar{Y}$ and δ, that adequately correlate all the experimental data (see Section 4), together with the asymptotic applicability of the formulation to the low Froude number releases of practical interest, amply justify using the following revised form of Eq. (10):

$$\rho_0 v_0 Y_\infty = \rho E(r,0)\frac{\partial Y}{\partial z}(r,0) \tag{11}$$

Eq. (11) was previously employed in a successful model of unsteady turbulent mixing of fresh water releases into brine [9].

In dilute salt solutions the mixture density ρ is related to the salt concentration ρ_s by

$$\rho = \rho_0 + k\rho_s \tag{12}$$

where k is a constant equal to 0.64 for NaCl solutions. Substituting Eq. (12) into Eq. (1) and carrying out the indicated differentiation gives

$$E = \ell^2\left(\frac{gk}{\rho}\frac{\partial \rho_s}{\partial z}\right)^{1/2} \simeq \ell^2\left(gk\frac{\partial Y}{\partial z}\right)^{1/2} \tag{13}$$

The second equality in Eq. (13) is an approximation obtained by moving ρ inside the differential and invoking the definition $Y = \rho_s/\rho$. This step is permissible for dilute solutions. The boundary condition given by Eq. (11), when combined with Eqs. (3), (5) and (13), becomes

$$\begin{aligned} v_0 Y_\infty &= \ell^2(gk)^{1/2}\left[\frac{\partial Y}{\partial z}(r,0)\right]^{3/2} \\ &= 6^{3/2}\beta^2(gk)^{1/2}\delta^{1/2}(Y_\infty - \bar{Y})^{3/2} \end{aligned} \tag{14}$$

where the small difference between ρ_0 and $\rho(r,0)$ is ignored.

Substituting Eq. (12) into Eq. (6) and again invoking the definition $Y = \rho_s/\rho$ gives

$$\frac{\partial P}{\partial z} = gk\rho(Y - Y_\infty) \tag{15}$$

Substituting Eq. (3) into Eq. (15) and integrating in the z direction then yields

$$P = gk\rho(Y_\infty - \overline{Y})\delta\left(\frac{\delta - z}{\delta}\right)^3 \tag{16}$$

while eliminating P between Eqs. (7) and (16) leads to

$$\frac{\mathrm{d}}{\mathrm{d}r}(r\bar{u}^2\delta) = \frac{rgk}{4}\frac{\mathrm{d}}{\mathrm{d}r}[(Y_\infty - \bar{Y})\delta^2] \tag{17}$$

To obtain useful closed-form solutions of the mixing layer equations, the radial geometry effects in Eq. (17) are assumed to be insignificant over the peripheral region $R_\mathrm{p} < r < R_0$. The quantity r in Eq. (17) can then be moved outside the derivative and the result integrated to get

$$\bar{u} = \frac{1}{2}[gk(Y_\infty - \bar{Y})\delta]^{1/2} \tag{18}$$

The integration constant in Eq. (18) is evaluated to be zero since both $\bar{u}$ and δ vanish at $r = R_0$. Eq. (8) may be integrated directly, resulting in

$$r\bar{u}\delta(Y_\infty - \bar{Y}) = \frac{1}{2}\, v_0 Y_\infty (R_0^2 - r^2) \tag{19}$$

Eqs. (14), (18) and (19) are sufficient to solve for $\delta(r)$, $\bar{u}(r)$, and $\bar{Y}(r)$:

$$\delta(r) = 6^{3/2}\beta^2\left(\frac{R_0^2 - r^2}{r}\right) \tag{20}$$

$$\bar{u}(r) = \frac{1}{2}(gkv_0 Y_\infty)^{1/3}\left(\frac{R_0^2 - r^2}{r}\right)^{1/3} \tag{21}$$

$$Y_\infty - \bar{Y}(r) = \frac{1}{6^{3/2}\beta^2}\left(\frac{v_0^2 Y_\infty^2}{gk}\right)^{1/3}\left(\frac{r}{R_0^2 - r^2}\right)^{1/3} \tag{22}$$

(Note from Eq. (22) that the solute mass fraction $|\bar{Y}| \to \infty$ as $r \to R_0$. This non-physical result is due to replacing $Y(r, 0)$ by Y_∞ in Eq. (10), as described previously.) Another useful variable is the total inward volumetric flow of fluid (released + entrained) within the mixing zone, namely

$$Q(r) = 2\pi r\delta\bar{u} \tag{23}$$

or, from Eqs. (20) and (21),

$$Q(r) = 6^{3/2}\pi\beta^2\,(gkv_0 Y_\infty)^{1/3}\left(\frac{R_0^2 - r^2}{r}\right)^{4/3} r \tag{24}$$

By ignoring r^2 compared with R_0^2 in Eq. (20) and eliminating r between this result and Eq. (24), one finds that $Q \sim \delta^{1/3}$ which agrees with theories and experiments on air entrainment into buoyant plumes above large-area pool fires [1]. Strictly speaking, Eqs. (20)–(22) and (24) are only valid in the region of the mixing layer that lies beneath the ambient fluid, that is in the radial segment $R_\mathrm{p} < r < R_0$ not covered by the plume (see Fig. 1). The volumetric fluid flow Q_p and the solute mass fraction Y_p may be related to $Q(R_\mathrm{p})$ and $\overline{Y}(R_\mathrm{p})$ by applying mixture and solute mass balances between the plume neck and the inner edge of the entrainment zone. (The portion of the mixing layer beneath the plume does not entrain ambient fluid.) It turns out that the inward radial flow $Q(R_\mathrm{p})$ into the region beneath the plume greatly exceeds the released (injected) flow $(R_\mathrm{p}/R_0)^2 Q_0$ so that the mass balances simplify to

$$Q_\mathrm{p} \simeq Q(R_\mathrm{p}) \quad \text{and} \quad Y_\mathrm{p} \simeq \overline{Y}(R_\mathrm{p}) \tag{25}$$

Once the neck radius R_p is known, the quantities Y_p and Q_p may be calculated. A theory for the determination of R_p is postponed to follow discussion of the equations that describe the plume (below). It can be shown that Eqs. (20)–(22) and (24) are readily converted to the corresponding dilute gas-system equations by making the substitutions

$$Y_\infty - \overline{Y}(r) = \overline{Y}_\mathrm{L}(r); \qquad k = \frac{M_\mathrm{H}}{M_\mathrm{L}} - 1; \quad \text{and} \quad Y_\infty = \frac{M_\mathrm{L}}{M_\mathrm{H}} \tag{26}$$

2.2. Plume

Consider the fully turbulent, circular plume that emanates from the top of the mixing layer discussed in the previous subsection. This plume rises from a 'perforation' in the mixing layer of finite size (radius R_p; see Fig. 1) under the influence of both gravity and the momentum supplied by the mixing layer. As the plume rises, it grows radially by entrainment of the surrounding ambient fluid (brine).

The conservation equations for solute mass, total mass, and momentum for an axisymmetric, isothermal buoyant plume are, respectively,

$$\frac{\mathrm{d}}{\mathrm{d}z}(R^2\rho_\mathrm{s} v) = 2R\rho_{\mathrm{s},\infty}u_\mathrm{e} \tag{27}$$

$$\frac{\mathrm{d}}{\mathrm{d}z}(R^2\rho v) = 2R\rho_\infty u_\mathrm{e} \tag{28}$$

$$\frac{\mathrm{d}}{\mathrm{d}z}(R^2\rho v^2) = g(\rho_\infty - \rho)R^2 \tag{29}$$

Eqs. (27)–(29) are based on uniform plug flow ('top

hat') profiles of velocity, $v(r,z)=v(z)$ as illustrated in Fig. 1, density, $\rho(r,z)=\rho(z)$, and solute concentration, $\rho_s(r,z)=\rho_s(z)$. The equations are subject to the initial conditions

$$v=v_p,\qquad \rho=\rho_p,\qquad \rho_s=\rho_{s,p},\qquad R=R_p\quad \text{at}\quad z=0 \tag{30}$$

The subscript p refers to conditions at the plume neck, and z is now measured from the neck. The quantities Q_p, ρ_p and $\rho_{s,p}$ can all be calculated from the above mixing layer theory, but R_p is still unknown.

To close the system of equations for the plume, an expression is required for the entrainment velocity u_e. It is appropriate to use the well-known entrainment equation of Morton et al. [10], as modified by Ricou and Spalding [11] for vastly different plume and ambient densities, ρ and ρ_∞, respectively:

$$u_e=E_0\left(\frac{\rho}{\rho_\infty}\right)^{1/2}v \tag{31}$$

where E_0 is the so-called entrainment coefficient. For buoyant plumes with plug flow profiles, Morton [12] was the first to suggest $E_0=0.12$. Note that the system of plume equations given above is not the analogue of the classical three equations of Morton et al. [10] for the vertical plume in a neutral atmosphere in that the Boussinesq approximation is not invoked in the present study. The similarity of the profiles $v(r,z)$, $\rho(r,z)$ and $\rho_s(r,z)$ at all heights above the neck is the main assumption made here, which perhaps can only be justified by its success in terms of the prediction of the neck radius R_p (see Section 4).

The problem of the isothermal non-Boussinesq plume can be reduced to the solution of the quadrature

$$Z=\int_1^\lambda \frac{dx}{[x^2+Fr_p-1]^{1/5}} \tag{32}$$

where λ is a dimensionless plume flow rate,

$$\lambda=\frac{\rho v R^2}{\rho_p v_p R_p^2}, \tag{33}$$

Z is a vertical dimensionless distance,

$$Z=\frac{2E_0}{R_p}\left(\frac{\rho_\infty}{\rho_p}\right)^{1/2}\frac{z}{Fr^{1/5}}=\left[\frac{20E_0^4 g\rho_\infty^2(\rho_\infty/\rho_p-1)}{R_p^4\rho_p^2 v_p^2}\right]^{1/5}z, \tag{34}$$

and Fr_p is a constant dimensionless plume-source Froude number

$$Fr_p=\frac{8E_0 v_p^2(\rho_\infty/\rho_p)^{1/2}}{5gR_p(\rho_\infty/\rho_p-1)} \tag{35}$$

For the singular case $Fr_p=1.0$, Eq. (32) can be solved analytically and the solution is

$$\lambda=\left(1+\frac{3}{5}Z\right)^{5/3} \tag{36}$$

For arbitrary Fr_p, Eq. (32) must be solved numerically. However, the possibility of representing the function $\lambda(Z)$ by an algebraic expression has been explored. The following approximate functional form represents a continuous transition between the solutions of Eq. (32) in the limits $Z\ll 1.0$ and $Z\to\infty$:

$$\lambda-1=0.4268Z^{5/3}\{1+1.4278Z^{-15/4}[(1.6Z+Fr_p{}^{4/5})^{5/4}-Fr_p]^{9/4}\}^{4/9} \tag{37}$$

The maximum error associated with Eq. (37) is less than 4.0%. The plume mixture density, velocity and radius are then obtained from

$$\rho=\frac{\rho_\infty}{1+(1/\lambda)[(\rho_\infty/\rho_p)-1]} \tag{38}$$

$$\frac{v}{v_p}=\frac{1}{\lambda}\left[\frac{1}{Fr_p}(\lambda^2-1)+1\right]^{2/5} \tag{39}$$

and

$$\frac{R}{R_p}=\left(\frac{\rho_p v_p\lambda}{\rho v}\right)^{1/2}=\frac{[(\rho_p/\rho_\infty)\lambda^2+(1-\rho_p/\rho_\infty)\lambda]^{1/2}}{[(1/Fr_p)(\lambda^2-1)+1]^{1/5}} \tag{40}$$

The plume model presented in this subsection accounts for a finite source area and combined plume momentum and buoyancy, and can be shown to agree with the available data on plume/jet dilution. The solutions for the water-into-brine plume are also valid for the light-gas into heavy-gas plume since ρ_H and $M_H/M_{L,p}$ for the gas system have the same meanings as ρ_∞ and ρ_∞/ρ_p, respectively, for the brine/water system.

2.3. Plume starting thickness

In order to apply the mixing layer and plume models to light fluid releases of practical interest the plume neck radius R_p must be determined. It is experimentally observed that, unlike the mixing layer boundary, the plume boundary tends to remain constant or expand with increasing height z (see Fig. 1). Thus it is

proposed that the mixing layer region changes to the plume region at that location where the volumetric flow supplied by the mixing layer is just sufficient to prevent the plume's cross section from shrinking. The idea is that if the flow continued to narrow after leaving the mixing layer it would not be in the plume, but would remain in the mixing layer.

The behavior of the plume boundary is characterized by Fr_p. This can be seen by differentiating Eq. (40) with respect to λ and setting the result equal to zero, to obtain the value of λ at which the plume radius is minimized. Since Z is a monotonic function of λ (see Eq. (32)), λ may be regarded as a transformed distance from the source. The plume radius is a minimum at the location λ that satisfies the following cubic equation:

$$\frac{6}{5}\frac{\rho_p}{\rho_\infty}\lambda^3+\frac{1}{5}\left(1-\frac{\rho_p}{\rho_\infty}\right)\lambda^2-2\frac{\rho_p}{\rho_\infty}(1-Fr_p)\lambda-\left(1-\frac{\rho_p}{\rho_\infty}\right)(1-Fr_p)=0 \tag{41}$$

By demanding that the plume necks down at the source $Z = 0$ (or equivalently, $\lambda = 1.0$), it is guaranteed that the plume thickness can only increase with height Z. Setting $\lambda = 1.0$ in Eq. (41) gives the value of the minimum or critical Froude number consistent with plume expansion

$$Fr_{p,cr}=\frac{4}{5(1+\rho_p/\rho_\infty)} \tag{42}$$

The notion that the transition from mixing layer to plume flow occurs when the source Froude number for the plume is given by Eq. (42) leads to the following condition at the neck (see Eq. (35)):

$$\frac{8E_0Q_p^2(\rho_\infty/\rho_p)^2}{5\pi^2 gR_p^5(\rho_\infty/\rho_p-1)}=\frac{4}{5(1+\rho_p/\rho_\infty)} \tag{43}$$

where for the brine/water system (see Eqs. (12) and (25))

$$\frac{\rho_\infty}{\rho_p}-1\simeq k(Y_\infty-Y_p)\simeq k[Y_\infty-\bar{Y}(R_p)] \tag{44}$$

Evaluating Eqs. (22) and (24) at $r = R_p$, combining the results with Eqs. (25), (43) and (44) and making the reasonable approximation $\rho_\infty = \rho_p$ in the numerator of the left side of Eq. (43) and in the denominator of the right side of Eq. (43), leads to

$$\frac{R_p}{R_0}=\frac{1}{[1+(4\cdot 6^{9/2}E_0\beta^6)^{-1/3}]^{1/2}} \tag{45}$$

Thus the ratio of the plume starting (neck) radius to the radius of the release disk is predicted to be only a function of the plume entrainment coefficient E_0 and the mixing-length-thickness proportionality coefficient β.

3. Experiments

Steady-state buoyant releases are investigated in an open rectangular tank having (inside) lateral dimensions of 0.892 m × 0.740 m, giving a cross sectional area of 0.66 m^2. The tank is 0.889 m high and is constructed of (transparent) acrylic plastic (see Fig. 2). A horizontal stainless steel 'partition' plate, with a circular hole cut to accommodate a porous release area, divides the tank into two compartments. The lower compartment is 0.127 m high and forms a supply plenum for fresh water, which is injected through the porous plate during the experiment. The upper 'mixing' compartment is 0.762 m high and initially contains brine. A porous plate (1.57 mm thick and 40 μm pore size) is positioned to cover the circular opening. Four different release configurations are employed during the course of the experiments: three centrally located openings with respective diameters 11.43, 22.86, and 35.56 cm and one off-center 22.86-cm opening. The minimum distance between the edge of the off-center opening and the front 'viewing' wall of the tank is 5.08 cm. Thus the off-center opening results in a 'near-wall release'.

During an experiment the fresh water is forced up through the release opening and forms a visible mixing zone in the brine reservoir above the opening. The mixing layer and to some extent the plume are visible

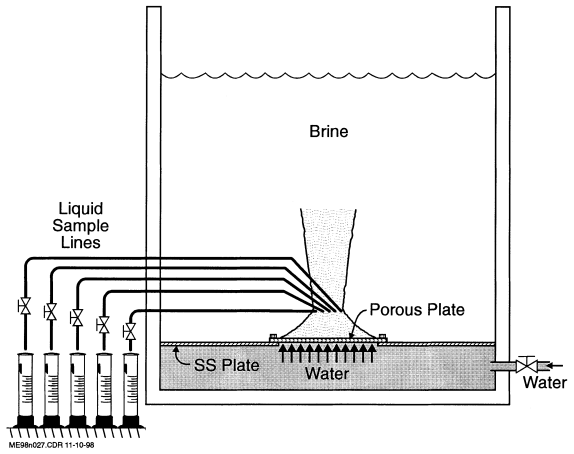

Fig. 2. Schematic diagram of the apparatus for studying density gradient-driven mixing above a circular release of buoyant fluid.

owing to refraction effects. A pressurized fresh water supply tank feeds water to the supply plenum at a steady rate. The time duration of the test and the volume of injected fresh water are measured so that the injection velocity can be determined. Uncertainty in the injection velocity is estimated to be $\pm 6\%$. The time duration of each test is sufficiently short that dilution of the bulk brine is negligible and a steady-state interpretation is deemed to be valid.

Videotape is used to record the shape of the mixing zone with the aid of a visualization grid, which is positioned vertically across the center of the composite mixing layer/plume. Liquid samples are taken at various positions in the mixing zone using an array of 500-ml graduated cylinders connected to 1/8-in. sampling lines. These samples are acquired relatively slowly (over about 1 min) so as to minimize disturbance of the flow within the mixing layer. In all cases the gravity flow of the sample into the collection cylinder is throttled down with a 1/8-in. ball valve. Sample density is directly measured using a hydrometer. A hydrometer is also used to measure the bulk brine density before and after each test. The hydrometers are readable with 95% confidence to within a brine specific gravity of 10^{-3}.

In terms of predicting the release fuel-gas concen-

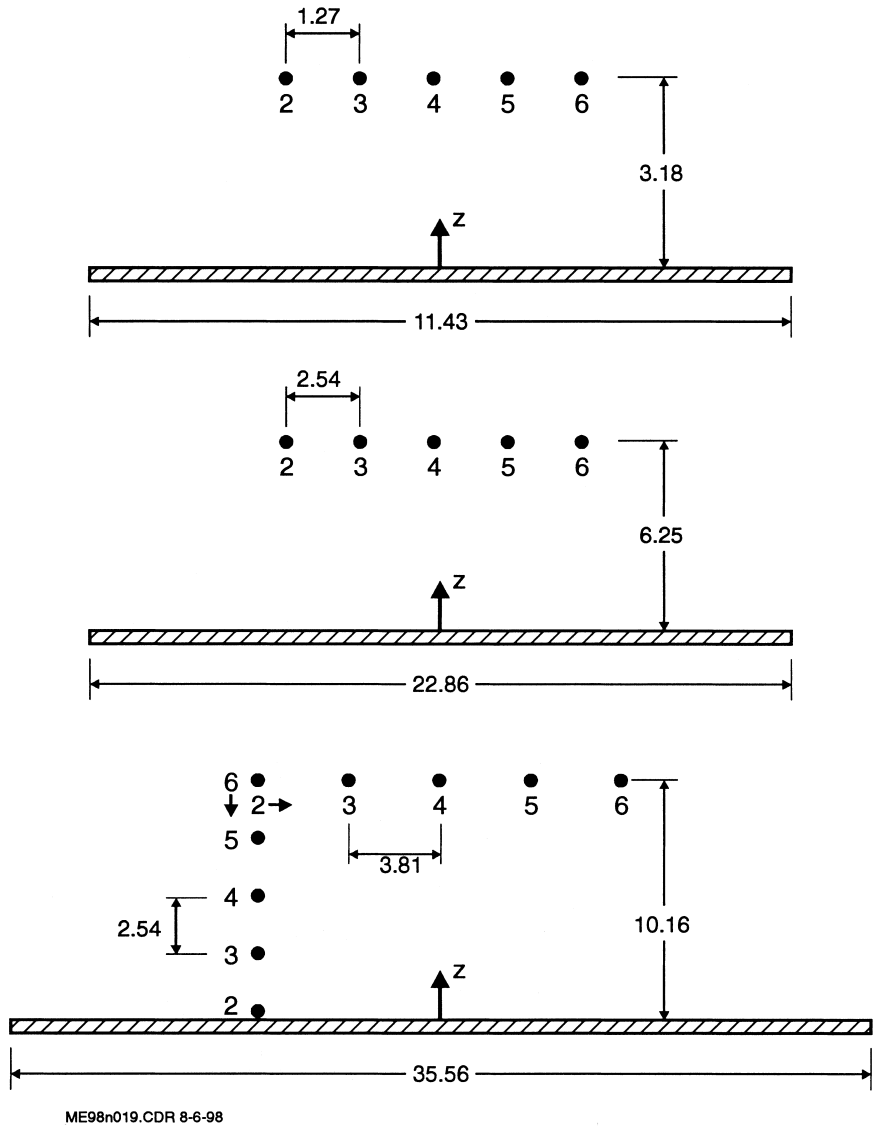

Fig. 3. Salt concentration sampling point locations above porous plates. All dimensions in centimeters.

tration in the dome region of a waste storage tank during a light fuel gas release, the neck region where the mixing layer meets the plume is of most interest. Thus, most of the salt concentration sampling is carried out with a horizontal array of five probes located equidistant from one another across this circular region (see Fig. 2). The sampling locations (r, z) above each of the openings are shown in Fig. 3. In the case of the 35.56-cm opening, in any one test sampling is done with either the horizontal array in the neck-in region or with a similar vertical array at $r = R_p$ (the inner radial boundary of the mixing layer). There is some ambiguity about the locations of the mixing regions and, therefore, about the placement of the probes. The positions of the probes shown in Fig. 3 are suggested by a combination of videotape observations of the mixing layer/plume boundaries and the theory, in particular Eq. (20). More details regarding the positioning of the probes are given in the next section. Raw data are available upon request.

4. Results and discussion

The normalized shapes of the mixing layer/plume composite as interpreted from the video images for six typical runs are shown in Fig. 4. Mixing layer/plume boundary data are acquired just after each porous disk is installed and prior to positioning the brine sampling lines. The mixing layer and plume boundaries are highly irregular. Considering the uncertainty associated with defining these boundaries (±20%, [9]) the experimental results suggest that the normalized shapes of the mixing layer and lower plume region are independent of the release size R_0, fluid injection rate v_0 and bulk (headspace) solute concentration Y_∞. This conclusion is consistent with the theoretical result given by Eq. (20). Eq. (20) with $\beta = 0.14$ represents a good fit of the measured mixing layer/plume boundary data (see Fig. 4). The videotape information indicates a constant plume thickness over the field of view of the camera. However, the salt concentration difference between the plume and surrounding brine is very small, which makes it difficult to observe the exact plume 'concentration' boundary.

The upper data points in Fig. 4 reveal that the measured radii of the plume R_p normalized by R_0 are in the range 0.35–0.55. Inserting $\beta = 0.14$ and $E_0 = 0.12$ into Eq. (45) gives a radius ratio $R_p/R_0 = 0.43$. This predicted plume radius ratio appears in Fig. 4 as the vertical line labeled 'plume boundary'. It follows from Eq. (20) that the horizontal mixing layer/plume boundary or neck is located a normalized distance $\delta/R_0 = 0.55$ above the release disk. These results were

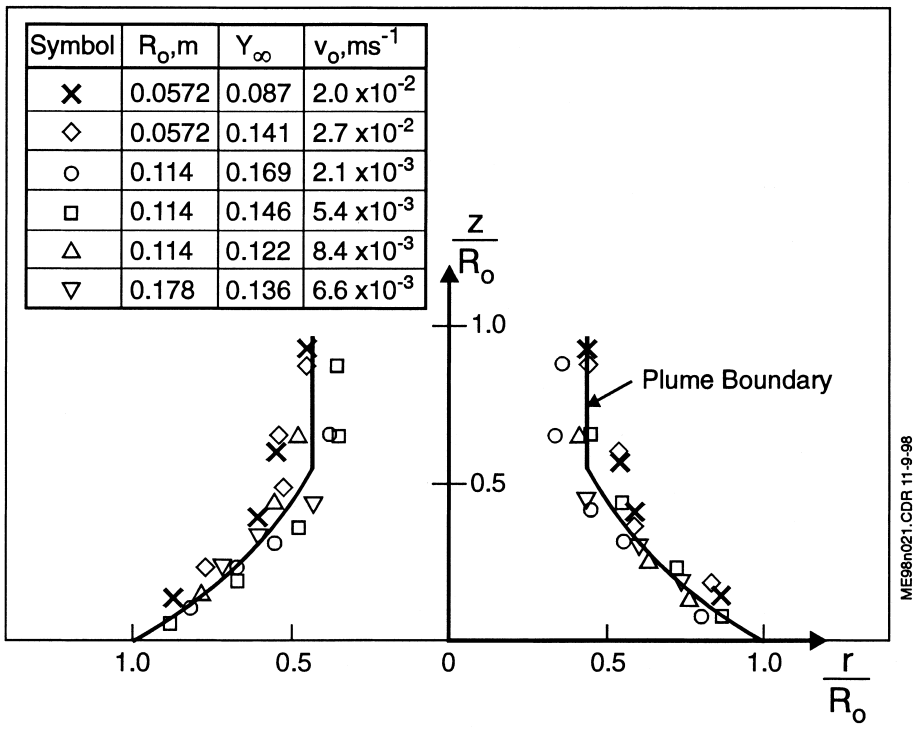

Fig. 4. Measured boundaries of mixing layer/plume composite, comparison with Eq. (20) and $\beta = 0.14$.

used to determine the boundary locations along which to position the salt concentration sampling probes (see Fig. 3).

Measured brine densities within the mixing layer and at the base of the plume (neck) are obtained by performing 72 separate experimental runs. Axial symmetry suggests that the brine densities at sampling positions 2 and 3 would be the same as the densities at positions 6 and 5, respectively (see Fig. 3), but this is not the case. Small differences are measured and are undoubtedly due to the fact that the mixing zone and the plume are not perfectly symmetric about the axis $r = 0$.

The measured brine density at sample location i is converted to salt mass fraction via the following form of the salt solution equation of state:

$$Y_i = \frac{1}{k}\left(1 - \frac{\rho_0}{\rho_i}\right) \tag{46}$$

which follows immediately from the definition of the solute mass fraction ($Y = \rho_s/\rho$) and Eq. (12). Eq. (22) predicts the local, vertically averaged salt concentration $\bar{Y}(r)$. The data from the vertical sampling points 2, 3, 4, 5 and 6 can be compared directly with the theory by taking the arithmetic average of the Y_is. The result $\bar{Y}(R_p)$ may be regarded as the average value over the vertical distance δ at the inner mixing layer boundary $r = R_p$. The data from the neck region sampling points 2, 3, ..., 6 must be 'radially averaged' to obtain the appropriate average value Y_p for comparison with the theory. Recall that the second equality in Eq. (25) states $\bar{Y}(R_p) \approx Y_p$. The radial averaging of the sampling point values Y_2, Y_3, and Y_4 can be accomplished by numerically evaluating the integral

$$Y_p = \frac{2}{R_2^2}\int_0^{R_2} rY\,dr \tag{47}$$

where R_2 is the radial location of sampling point 2. To circumvent the zero integrand difficulty at the centrally located sampling point 4 (where $r = 0$), the integration variable is transformed via $\xi = (r/R_2)^2$. Hence, $Y_p = \int_0^1 Y(\xi)d\xi$, where $Y(0) = Y_4$, $Y(1/4) = Y_3$ and $Y(1) = Y_2$. Simpson's rule is used to evaluate the integral for the unequally spaced pivotal points $\xi = 0$, 1/4, 1.0. Since the sample densities at positions 5 and 6 are not quite the same as those at positions 2 and 3, the radial averaging technique is repeated for sampling points 4, 5, and 6, and the arithmetic average of the two radially averaged Y_p values are used to compare with the theory.

The salt concentrations inferred from the measured brine densities within the mixing zone and in the source region of the plume are plotted in Fig. 5 in a form suggested by Eq. (22) with $r = R_p = 0.43R_0$; namely

$$Y_\infty - \bar{Y}(R_p) \simeq Y_\infty - Y_p = \frac{0.055}{\beta^2}\left(\frac{v_0^2 Y_\infty^2}{gkR_0}\right)^{1/3} \tag{48}$$

The data points are positioned using a mixing-length-thickness proportionality coefficient $\beta = 0.14$, as already inferred from the plume/mixing zone profile data (see Fig. 4). The average salt mass fraction data in the source region of the plume above the 0.178-m radius release are represented in Fig. 5 by the open squares, while the dark squares represent the average salt mass fraction $\bar{Y}(R_p)$ data at the inner radial boundary of the 0.178-m radius mixing layer. The circles and the xs in Fig. 5 pertain to the center and near-wall releases, respectively. The level of uncertainty for the local salt concentration relative to Y_∞ is $\pm 30\%$. While on the average the near-wall release results lie below the center release data, the difference is within the data uncertainty range and should not be regarded as significant. Clearly the choice $\beta = 0.14$ results in a conservative correlation since most of the $Y_\infty - \bar{Y}(R_p)$ data lie below the curve. Recall that there is a direct analogy between $Y_\infty - \bar{Y}(r)$ for solute salt and Y_L for the gas system. Thus a good correlation of the brine/water $Y_\infty - \bar{Y}(r)$ data is equivalent to useful predictions of the light (fuel) gas concentration $\bar{Y}_L(r)$.

The value $\beta = 0.14$ required to bring the theory and the measurements together is somewhat different than the value $\beta = 0.164$ inferred from a previous laboratory study of buoyant releases [9]. Two possible reasons for this rather minor discrepancy are (i) the present problem involves steady-state mixing while the previous study was concerned with transient mixing and (ii) the present theoretical approach is based on the approximate integral technique while an exact similarity solution was obtained for the transient mixing problem. It is worth noting that a small increase in the value of β would provide a better fit of the data with the theory than is displayed in Fig. 5.

5. Summary

This study examines the mixing pattern above a steady, buoyant release of fresh water into brine. The fresh water is injected at low velocity, through a porous disk at the bottom of a large tank of heavier brine. This system is used to represent the axisymmetric release of light fuel gas into overlying air. Visualization of the flow shows that a concentration boundary- or mixing-layer develops that is directed inward above the release surface. Near the center of the release surface the mixing layer turns upward and changes to a vertical plume flow. Approximate inte-

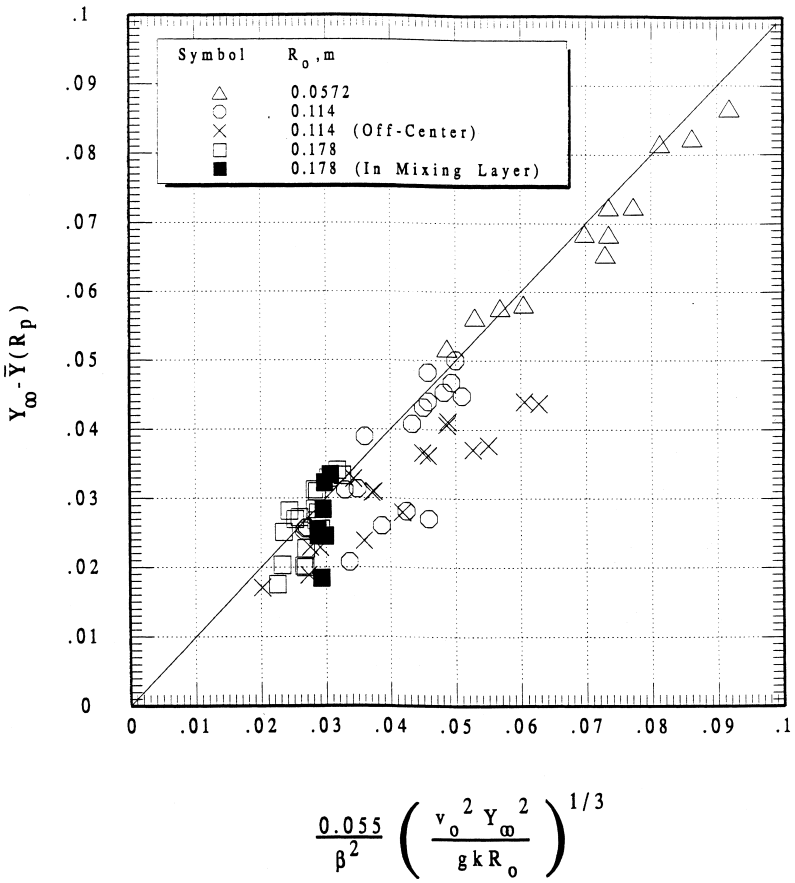

Fig. 5. Measured salt mass fractions compared with Eq. (48).

gral-profile type solutions of the concentration boundary layer equations for turbulent flow are combined with the governing equations for vertical plume flow to determine the gross properties (shape and average solute salt concentrations) of the mixing layer. The crucial vertical diffusion component of the concentration boundary layer equations is related to the local concentration gradient and characteristic mixing length by an equation first proposed by Baird and Rice [3] for gravity-driven mixing in high-aspect ratio columns. Reasonable correlation of the brine-water data is obtained by assuming that the mixing length is proportional to the local thickness of the mixing layer. Apparently, the gravity-generated turbulent structure in wide mixing layers is the same kind that exists in tall vertical mixing columns.

References

[1] M.A. Delichatsios, Air entrainment into buoyant jet flames and pool fires, in: P.J. DiNeno (Ed.), SFPE Handbook of Fire Protection Safety, Natural Fire Protection Association, Quincy, MA, 1988, pp. 306–314.
[2] M. Al-Arahi, M.K. El-Riedy, Natural convection heat transfer from isothermal horizontal plates of different shapes, Int. J. Heat Mass Transfer 19 (1976) 1399–1404.
[3] M.H.I. Baird, R.G. Rice, Axial dispersion in large unbaffled columns, Chem. Eng. J. 9 (1975) 171–174.
[4] T.L. Holmes, A.E. Karr, M.H.I. Baird, Effect of unfavorable continuous phase density gradient on axial mixing, Am. Inst. Chem. Eng. J. 37 (1991) 360–366.
[5] M.H.I. Baird, N.V. Rama Rao, Axial mixing in a reciprocating plate column in presence of very small density gradients, Am. Inst. Chem. Eng. J. 37 (1991) 1019–1026.
[6] M.H.I. Baird, K. Aravamudan, N.V. Rama Rao, J. Chadam, A.P. Peirce, Unsteady axial mixing by natural convection in a vertical column, Am. Inst. Chem. Eng. J. 38 (1992) 1825–1834.
[7] M. Epstein, Buoyancy-driven exchange flow through small openings in horizontal partitions, J. Heat Transfer 110 (1988) 885–893.
[8] G.C. Gardner, Motion of miscible and immiscible fluids in closed horizontal and vertical ducts, Int. J. Multiphase Flow 3 (1977) 305–318.

[9] M. Epstein, J.P. Burelbach, Transient vertical mixing by natural convection in a wide layer, Int. J. Heat Mass Transfer 43 (2000) 321–325.
[10] B.R. Morton, G.I. Taylor, J.C. Turner, Turbulent gravitational convection from maintained and instantaneous sources, Proc. R. Soc. London Ser. A 234 (1956) 1–23.
[11] F.B. Ricou, D.B. Spalding, Measurements of entrainment of axisymmetrical turbulent jets, J. Fluid Mech. 11 (1961) 21–32.
[12] B.R. Morton, Forced plumes, J. Fluid Mech. 5 (1959) 151–163.